JCTC Journal of Chemical Theory and Computation

Article

pubs.acs.org/JCTC

Quasi-diabatic States from Active Space Decomposition

Shane M. Parker* and Toru Shiozaki*

Department of Chemistry, Northwestern University, 2145 Sheridan Rd., Evanston, Illinois 60208, United States

ABSTRACT: We present *ab initio* theory and efficient algorithms for computing model Hamiltonians of excited-state dynamics in the quasi-diabatic representation. The method is based on a recently developed multiconfiguration electronic structure method, called the active space decomposition method (ASD), in which quasi-diabatic basis states are constructed from physical fragment states. An efficient tree-based algorithm is presented for computing and reusing intermediate tensors appearing in the ASD model. Parallel scalability and wall times are reported to attest the efficiency of our program. Applications to electron, hole, and triplet energy transfers in molecular dimers are presented, demonstrating its versatility.

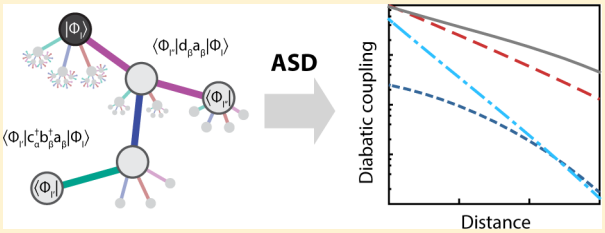

1. INTRODUCTION

Most work in electronic structure theory to date has been devoted to establishing an accurate and efficient method with which one obtains the electronic eigenstates that diagonalize molecular electronic Hamiltonians under the Born−Oppenheimer approximation.[1] These states are termed adiabatic states, and are uniquely defined. This adiabatic representation of electronic structure is often used when calculating time-averaged or time-independent properties, such as excitation energies and oscillator strengths from the ground state within the linear response approximation.[2] Recent years saw electronic structure simulations of an entire protein described by very accurate coupled-cluster methods,[3] and those of small molecules simulated to precision far below experimental limits.[4,5]

On the other hand, dynamical processes in chemistry are often explained in the diabatic representation, which is formally defined as a set of states between which the derivative coupling $\langle \Psi_I | d/dR_{\mathrm{nuc}} | \Psi_J \rangle$ is zero. The diabatic states allow us to interpret the dynamical processes in an intuitive way. For instance, exciton dynamics in the excited states are described by local states in real space, in which excitons hop between sites. Even though, strictly speaking, diabatic states do not exist in general,[6] there are several approaches that calculate quasi-diabatic states from adiabatic states obtained in quantum chemical calculations: some are based on diagonalization of a property matrix,[7] and others are based on wave function analyses.[8−10] The latter is nevertheless limited to few atom systems, since one needs to connect two geometries by reaction paths on hypersurfaces, a task that is not straightforward for systems containing a few tens of atoms. Diabatization based on the Boys localization has been recently proposed by Subotnik and co-workers.[11,12]

Another route to diabatic states is to directly compute them using electronic structure methods that impose constraints to the properties of the states. Among others, constrained density functional theory (DFT), first developed by Dederichs et al.[13] and recently revived by Van Voorhis and co-workers,[14,15] has been used to obtain quasi-diabatic states within the DFT framework. The diabatic couplings (i.e., off-diagonal Hamiltonian matrix elements between diabatic states) can be computed by approximating excited-state wave functions by a linear combination of a few Slater determinants.[16] Molecular orbital valence bond (MOVB) methods[17,18] likewise directly compute diabatic states that are defined by valence bond structures and couplings between them. Similarly, active space wave function methods have been used to compute quasi-diabatic states[19,20] on the basis of the restricted active space state interaction (RASSI) developed by Malmqvist.[21]

Yet another approach for direct computation of diabatic states is the renormalized excitonic methods (REM) developed by Malrieu and co-workers,[22] later extended by Ma and co-workers,[23−25] in which the parameters in the Frenkel exciton model for excited states of molecular aggregates[26] are computed using DFT. The REM method has successfully parametrized the model Hamiltonians for energy transfers.[25] This method has its origin in the real-space renormalization group approach to Hamiltonians—the contractor renormalization group[27,28] or real-space renormalization group with effective interactions.[29] In their method, excitonic states of molecular aggregates are expressed as $\Psi = \Phi_J^* \Pi_{I \neq J} \Phi_I$, where Φ_I and Φ_J^* are the ground and excited states of fragment I and J that are computed by DFT and time-dependent DFT (TD-DFT), respectively. Note that only one-exciton can be described in their model, because of the use of TD-DFT states that are not compact.

In this work, we present a novel many-body electronic structure method that directly provides quasi-diabatic states for excited-state dynamics, called the active space decomposition (ASD) method,[30] in which we use molecular geometry information to decompose the active spaces. The ASD

Received: June 2, 2014
Published: July 15, 2014

   dx.doi.org/10.1021/ct5004753 | J. Chem. Theory Comput. 2014, 10, 3738−3744

approach is potentially exact when complete sets of fragment states are included; thus, it can be seen as an extension of REM to many-body wave function that is applicable to multiple exciton and charge-separated states. The resulting adiabatic wave functions are described in terms of a linear combination of products of fragment states. The structure of the wave functions defines quasi-diabatic states that are relevant to chemical processes, as we have demonstrated earlier for model Hamiltonians of singlet fission processes.[31] Efficient parallel algorithms are presented for computing quasi-diabatic states using the ASD method. The connections to product state ansätze (such as matrix product state and tensor product state wave functions) will be discussed. The method will be applied to electron, hole, and triplet energy transfer processes. All the programs have been interfaced to BAGEL[32] and are publicly available.

2. THEORY

Active Space Decomposition. In our model, the active space wave function of a system consisting of two distinct fragments, A and B, are expressed in the product basis

$$|\Psi\rangle = \sum_{IJ} C_{IJ}|\Psi_{IJ}\rangle \tag{1}$$

$$|\Psi_{IJ}\rangle = |\Phi_I^A\rangle|\Phi_J^B\rangle \tag{2}$$

in which orbitals in fragment A and B are assumed to be orthogonal, and $|\Phi_I^A\rangle$ are monomer states that are orthogonal with each other:

$$\langle\Phi_I^A|\Phi_J^A\rangle = \delta_{IJ} \tag{3}$$

$$\langle\Phi_I^A|\Phi_J^B\rangle = 0. \tag{4}$$

Note that $|\Psi_{IJ}\rangle$ is properly antisymmetrized with respect to interchanges of electrons in fragment A and B. These orthogonality conditions of orbitals and states are essential to arriving at simple and efficient working equations.

We have recently shown[30] that, using this basis, Hamiltonian matrix elements can be computed as

$$\langle\Psi_{I'J'}|\hat{H}|\Psi_{IJ}\rangle = (-1)^{\phi}\sum_{\zeta\eta}\Gamma_{\zeta}^{A,I'I}h_{\zeta,\eta}\Gamma_{\eta}^{B,J'J} \tag{5}$$

in which we have used a rearranged Hamiltonian and an intermediate tensor Γ, respectively defined as

$$\hat{H} = (-1)^{\phi}\sum_{\zeta\in A}\sum_{\eta\in B}h_{\zeta,\eta}\hat{E}_{\zeta}\hat{E}_{\eta} \tag{6}$$

$$\Gamma_{\zeta}^{A,I'I} = \langle\Phi_{I'}^A|\hat{E}_{\zeta}|\Phi_I^A\rangle \tag{7}$$

Here, ζ and η are the collections of indices associated with fragment A and B, respectively, and $(-1)^{\phi}$ is a phase factor due to the rearrangement. The Hamiltonian is, in practice, expressed as a sum of terms with different numbers of operators acting on A and B:

$$\begin{aligned}\hat{H} = {} & \hat{H}_{AA,AA} + \hat{H}_{BB,BB} + 2\hat{H}_{AA,BB} + \hat{H}_{AB,AB} + \hat{H}_{BA,BA} \\ & + 2\hat{H}_{BA,AB} + 2\hat{H}_{AA,AB} + 2\hat{H}_{AA,BA} + 2\hat{H}_{AB,BB} \\ & + 2\hat{H}_{BA,BB}\end{aligned} \tag{8}$$

The individual terms are, for instance,

$$\hat{H}_{BA,AB} = \frac{1}{2}\sum_{\rho\sigma}\sum_{i_Bj_Ak_Al_B}(i_Bj_A|k_Al_B)a_{i_B\rho}^{\dagger}a_{k_A\sigma}^{\dagger}a_{l_B\sigma}a_{j_A\rho} \tag{9}$$

where orbitals j_A and k_A belong to fragment A, and i_B and l_B belong to B. By regrouping the operators, it can be written as

$$\hat{H}_{BA,AB} = -\frac{1}{2}\sum_{\rho\sigma}\sum_{i_Bj_Ak_Al_B}(i_Bj_A|k_Al_B)(a_{k_A\sigma}^{\dagger}a_{j_A\rho})(a_{i_B\rho}^{\dagger}a_{l_B\sigma}) \tag{10}$$

which is in the form of eq 6. Other terms are similarly defined. See ref 30 and its supporting information for details.

As apparent from eq 5, the Hamiltonian matrix elements can be computed without explicit construction of total wave functions, allowing us to use any monomer active wave functions for which the transition density matrices in eq 5 can be computed. This is in stark contrast to occupation restricted active space models such as the quasi-complete active space method of Nakano and Hirao[33] or any other models.[34−36] Apart from orthogonality, the choice of basis states is arbitrary as long as computation of eq 7 is feasible. Active space wave functions [such as complete active space (CAS)[1] and those with occupation restrictions[34−36]] are natural choices, since eq 7 can be computed by the standard algorithms for reduced density matrices. The use of excited-state wave functions from linear response (such as TD-DFT and equation-of-motion coupled cluster) is not recommended as there is no efficient way of evaluating eq 7, unless one introduces a restriction that either of I or I' is always the ground state.[22,24] Hereafter, we adhere to the CAS wave functions, unless otherwise stated.

These equations resemble those used in the density matrix renormalization group (DMRG) method,[37−40] in which diagonalization within the superblocks in the sweep algorithm is performed similarly to eq 5. In fact, as pointed out by others,[41] the standard *ab initio* DMRG code can emulate our ASD model when CAS wave functions are used as a monomer basis. An optimized implementation of ASD, however, allows for adaptation of various active space models for monomer basis, as have been shown elsewhere.[31] Therefore, our model can be seen as a low-entanglement representation[42] of the total wave function using *a priori* chemical knowledge of the system. The comparisons of ASD and matrix-product state (MPS) ansätze are summarized in Figure 1. The slight empiricism due to manual partitioning of the system is compensated by the potential exactness of the model that allows us to control the accuracy of the decomposition. Among the advantages of ASD over the standard DMRG methods is that one can use configuration-based approximations (such as restricted active space models, or RAS[34]) for monomer states. In this regard, the

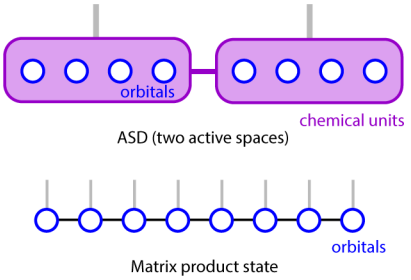

Figure 1. Comparisons of the active space decomposition (ASD) wave functions and matrix-product wave functions used in DMRG.

dx.doi.org/10.1021/ct5004753 | J. Chem. Theory Comput. 2014, 10, 3738−3744

ASD method is a hybrid of MPS and traditional quantum chemistry.

Procedurally, a calculation using the ASD method begins with a Hartree−Fock calculation of the total system to obtain canonical molecular orbitals. Then, the full set of canonical molecular orbitals are localized and assigned to fragments such that each fragment has a localized orthogonal set of orbitals (and all orbitals on fragment A are orthogonal to all orbitals on fragment B). Next, a set of fragment wave functions are computed using either CAS or RAS fragment wave functions. For each *type* of fragment state desired (i.e., singlet, triplet, anion, cation, etc.), M states are computed and stored, always with maximum spin projection ($m_s = S$). The rest of the spin manifold for each type of state ($m_s \neq S$) is computed by applying the spin lowering operator. Finally, transition density matrices between fragment states are computed and the dimer space is diagonalized to find eigenstates.

Diabatic Model Hamiltonians. In what follows, we apply ASD to compute diabatic model Hamiltonians of charge and energy transfer processes in molecular dimers, where the two fragments are defined as the two monomers comprising the dimer. The diabatic model Hamiltonians are computed by first identifying model states and then computing the exact matrix elements in the basis of these model states. The basis states in which we expand the dimer wave function are, by construction, diabatic in the sense that each monomer state in each dimer basis has a well-defined charge and spin. In other words, the $|\Phi^X\rangle$ in eq 2 are eigenstates of the spin angular momentum operator, $(\hat{S}^X)^2$, the spin-projection operator, $\hat{S}^X_z$, and the electron number operator, $\hat{N}^X$, all confined to act on monomer X. Therefore, we can straightforwardly define diabatic subspaces as sets of dimer basis states in which monomer A and B have the same charge (q_A and q_B) and spin (S_A and S_B). Then, diabatic model states are found by diagonalizing the diabatic sub-block of the Hamiltonian, i.e., by diagonalizing

$$\hat{H}_{\text{diabatic}} = \hat{P}_{\text{diabatic}}\hat{H}\hat{P}_{\text{diabatic}} \tag{11}$$

where $\hat{P}_{\text{diabatic}}$ is the projector onto the quasi-diabatic states of interest.

For example, consider the hole transfer process shown schematically in Figure 2:

$$A^+ + B \rightarrow A + B^+$$

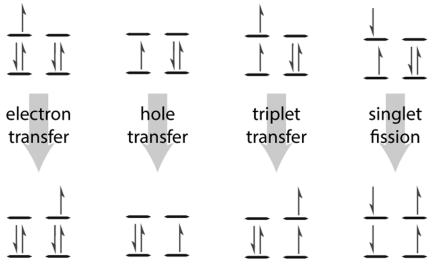

Figure 2. Depictions of electron transfer (ET), hole transfer (HT), triplet excitation transfer (TT), and singlet fission (SF).

The following two diabatic dimer states describe this process:

$$|\Psi_{0+}\rangle = \sum_{IJ} C_{IJ}^{0+}|\Phi^A_{I,0,0}\rangle|\Phi^B_{J,+1,1/2}\rangle \tag{12}$$

$$|\Psi_{+0}\rangle = \sum_{IJ} C_{IJ}^{+0}|\Phi^A_{I,+1,1/2}\rangle|\Phi^B_{J,0,0}\rangle \tag{13}$$

where $|\Phi^X_{I,q,S}\rangle$ is the Ith eigenstate of monomer X that has charge q and spin S. To find $|\Psi_{0+}\rangle$, we compute the lowest lying eigenstates of the subspace spanned by the products of all neutral singlet monomer A states and all cationic doublet monomer B states, $\{|\Phi^A_{I,0,0}\rangle\} \otimes \{|\Phi^B_{J,+1,1/2}\rangle\}$. $|\Psi_{+0}\rangle$ is computed similarly. The model Hamiltonian for the direct electron transfer is then computed as

$$H^{\text{model}} = \begin{pmatrix} \langle\Psi_{0+}|\hat{H}|\Psi_{0+}\rangle & \langle\Psi_{0+}|\hat{H}|\Psi_{+0}\rangle \\ \langle\Psi_{+0}|\hat{H}|\Psi_{0+}\rangle & \langle\Psi_{+0}|\hat{H}|\Psi_{+0}\rangle \end{pmatrix} \tag{14}$$

For mediated processes an effective model Hamiltonian must be formed. Examples of such processes include triplet energy transfer[43] and singlet fission[44] both of which are mediated by charge-transfer states. Appealing to the symmetrized Bloch equation[45] (or, more specifically, to quasi-degenerate perturbation theory[46] to second order), one arrives at

$$\tilde{H}_{KK'} = H_{KK'} + \frac{1}{2}\sum_{Z\notin\text{model}} \langle\Psi_K|\hat{H}|Z\rangle\langle Z|\hat{H}|K'\rangle \times \left(\frac{1}{E_K - E_Z} + \frac{1}{E_{K'} - E_Z}\right) \tag{15}$$

where the sum is over select (or, possibly, all) dimer states that are not in the diabatic spaces.

3. ALGORITHMS AND IMPLEMENTATIONS

Tree-Based Algorithm for Γ Intermediates. Our algorithm for computing the Γ tensors (eq 7) makes use of common intermediates. This is accomplished by mapping the full set of desired tensor elements onto a series of tree structures in which the edges (branches) represent second quantization operators and the nodes represent sets of CI vectors (see Figure 3). All of the tensor elements involving the same ket vector (e.g., $|\Phi_I\rangle$) are collected into a single tree in which said ket vector forms the root node. All other nodes (i.e., nonroot nodes) contain *sets* of bra vectors (e.g., $\{\langle\Phi_J|\}$). An individual tensor element is expressed as a path between the root node and some other node: starting from the ket vector (root node), each edge applies an operator and the terminal node (of the path) applies a bra vector; that is, an inner product is taken with the CI vectors at the terminal node of the path. Since, at most, three operators need to be applied, the maximum height of the tree is 4. Intermediate nodes along the

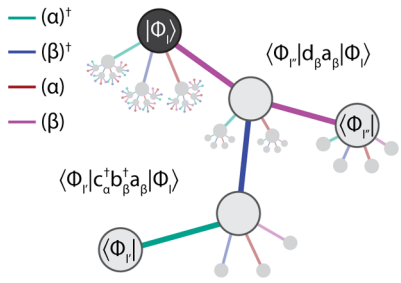

Figure 3. Sample skeleton tree for the computation of the transition density matrices.

dx.doi.org/10.1021/ct5004753 | J. Chem. Theory Comput. 2014, 10, 3738−3744

path have no physical meaning; only the root node and the terminal node of the path have meaning.

The trees are initially constructed in terms of a skeleton tree that specifies the *types* of edges (operators) that are needed. There are four types of edges in the skeletons, one for each type of second quantization operator: $(\alpha)^\dagger$, $(\beta)^\dagger$, (α), and (β). The full trees are generated from the skeletons by replacing each skeleton edge with one real edge per active orbital. Thus, the pair of skeleton edges $(\alpha)^\dagger(\alpha)$ represents n_{act}^2 real edges where n_{act} is the number of active orbitals on the monomer. A sample skeleton tree is shown in Figure 3.

Using the tree, the elements of the Γ tensors are computed analogously to a parallel depth-first search within each tree. In our implementation, each CI vector is distributed across all of the message passing interface (MPI) processes. Thus, before computing the matrix elements within a single tree, a gather operation is performed on the ket vector so that each MPI process has a local copy, referred to here as $|\Xi_0\rangle = |\Phi_I\rangle$, where $|\Phi_I\rangle$ is the ket vector associated with the root of the current tree. Furthermore, each MPI process stores a local copy of each transition density matrix, $\Gamma_{\xi}^{IJ,[n]}$, where, hereafter, $[n]$ denotes MPI process n.

The tree is traversed in parallel. Each step (moving from one "source" node to another "target" node in the tree) in the traversal is carried out by first applying a second quantization operator to form an intermediate, computing the inner product between the intermediate and all bra vectors held on the target node, and repeating this process for each child of the target node. One intermediate, $|\Xi_l\rangle$, is stored per level of the tree where a node's level, l, is defined as the number of edges between the node and the root. The intermediates are formed by applying a second quantization operator (specified by the edge in the tree) to the previous level's intermediate, $|\Xi_l\rangle = \hat{a}_{p,\sigma}|\Xi_{l-1}\rangle$. The action (change of occupation) of a single creation or annihilation operator on a Slater determinant and the phase [ϕ in $|I'\rangle = (-1)^{\phi}\hat{a}|I\rangle$, where $|I\rangle$ and $|I'\rangle$ are Slater determinants] are computed using bit-wise operations through the bitset class of the C++ standard. Then, inner products with all CI vectors contained in the node are computed and stored in the appropriate (local) transition density matrix. Since the bra vectors held at each node of the tree are distributed across MPI processes, the inner product is taken within each MPI process,

$$\Gamma_{\xi}^{IJ,[n]} = \sum_{I\in[n]} \langle\Phi_J|I\rangle\langle I|\Xi_l\rangle \tag{16}$$

and later summed across all the processes as

$$\Gamma_{\xi}^{IJ} = \sum_{n} \Gamma_{\xi}^{IJ,[n]} \tag{17}$$

The standard MPI_Allreduce is used for summation.

As a simplest example, we show an algorithm for computing

$$\Gamma_{q_\alpha}^{IJ} = \langle\Phi_J|\hat{a}_{q,\alpha}|\Phi_I\rangle \tag{18}$$

$$\Gamma_{p_\alpha,q_\alpha}^{IJ'} = \langle\Phi_{J'}|\hat{a}_{p,\alpha}^\dagger\hat{a}_{q,\alpha}|\Phi_I\rangle \tag{19}$$

which are obtained along the same path in the tree. First, $|\Phi_I\rangle$ is replicated and stored locally as $|\Xi_0\rangle$, and the first intermediate

$$|\Xi_1\rangle = \hat{a}_{q,\alpha}|\Xi_0\rangle \tag{20}$$

is computed. The inner product with the locally available portion of the bra vector, $\langle\Phi_j^{[n]}|$, is then formed,

$$\Gamma_{q_\alpha}^{IJ,[n]} = \langle\Phi_J^{[n]}|\Xi_1\rangle \tag{21}$$

Next, using the above $|\Xi_1\rangle$ intermediate, the second intermediate $|\Xi_2\rangle$ and $\Gamma_{p_\alpha q_\alpha}^{IJ',[n]}$ are likewise computed as

$$|\Xi_2\rangle = \hat{a}_{p,\alpha}^\dagger|\Xi_1\rangle \tag{22}$$

$$\Gamma_{p_\alpha,q_\alpha}^{IJ',[n]} = \langle\Phi_{J'}^{[n]}|\Xi_2\rangle \tag{23}$$

Finally, transition density matrices are summed as in eq 17. For a more-detailed description of the algorithm for traversal of the Γ trees, see Figure 4.

- Each node, $\mathcal{N}$, contains
  - a set of CI vectors: $\{|\Phi_I\rangle\}$ for root, $\{\langle\Phi_J|\}$ for others
  - a set of outbound edges (branches) connecting it to other nodes
- Each $\Phi_{I/J}$ is distributed across compute nodes
- Each Ξ_ℓ is stored locally within a compute node
- $\langle\Phi_J|\Xi_\ell\rangle$ is a partial inner product over the portions of Φ_J stored within the given compute node

foreach $|\Phi_I\rangle$ **do**
  $\mathcal{N}_0 \leftarrow$ root node
  $|\Xi_0\rangle \leftarrow$ Gather distributed $|\Phi_I\rangle$ vector into local vector
  foreach in parallel *outbound edge* **a** *from root node,* $\mathcal{N}_0$ **do**
    $\mathcal{N}_A \leftarrow$node connected to root via **a**
    $|\Xi_1\rangle \leftarrow \hat{\mathbf{a}}|\Xi_0\rangle$
    foreach $\langle\Phi_J|$ *in* $\mathcal{N}_A$ **do**
      $\Gamma_{a}^{JI,[n]} = \langle\Phi_J|\Xi_1\rangle$
    foreach *outbound edge* **b** *from node* $\mathcal{N}_A$ **do**
      $\mathcal{N}_B \leftarrow$ node connected to $\mathcal{N}_A$ via **b**
      $|\Xi_2\rangle \leftarrow \hat{\mathbf{b}}|\Xi_1\rangle$
      foreach $\langle\Phi_J|$ *in* $\mathcal{N}_B$ **do**
        $\Gamma_{ba}^{JI,[n]} = \langle\Phi_J|\Xi_2\rangle$
      foreach *outbound edge* **c** *from node* $\mathcal{N}_B$ **do**
        $\mathcal{N}_C \leftarrow$ node connected to $\mathcal{N}_B$ via **c**
        $|\Xi_3\rangle \leftarrow \hat{\mathbf{c}}|\Xi_2\rangle$
        foreach $\langle\Phi_J|$ *in* $\mathcal{N}_C$ **do**
          $\Gamma_{cba}^{JI,[n]} = \langle\Phi_J|\Xi_3\rangle$
foreach Γ **do** Allreduce;

Figure 4. Sketch of the algorithm used to compute Γ matrices.

We note that there is a large amount of flexibility in the ordering of the second quantization operators. One could, in principle, optimize the order of the application of the operators in order to better make use of common intermediates, minimize the size of unnecessary intermediate tensors, or maximize parallel efficiency. This would be equivalent to the optimization of a directed acyclic graph. In practice, however, we expect the gain from this to be minor compared to the gain from parallelization.

Parallel Algorithms and Timing. The program is parallelized using the hybrid MPI/thread approach. In addition to the parallel Γ tree algorithm in the previous section, construction of closed-Fock operator and configuration interaction in the active space are both parallelized.

The three-index density fitting integrals are distributed by the range of auxiliary fitting functions, i.e., $(\{\gamma\}|rs)$ with $\gamma_{\mathrm{begin}} \le \gamma \le \gamma_{\mathrm{end}}$. In our code, γ_{begin} and γ_{end} on each MPI process is chosen to be at the basis shell boundaries. Here $\{\cdots\}$ denotes that the code is parallelized using these indices. The Fock matrix is computed by the standard algorithm,

dx.doi.org/10.1021/ct5004753 | J. Chem. Theory Comput. 2014, 10, 3738−3744

$$(\{\gamma\}|is) = \sum_r (\{\gamma\}|rs)C_{ri} \tag{24}$$

$$(\gamma|\{is\}) = (\{\gamma\}|is) \qquad \text{collective} \tag{25}$$

$$(\tilde{\gamma}|\{is\}) = \sum_\delta (\mathcal{J}^{-1/2})_{\gamma\delta}(\delta|\{is\}) \tag{26}$$

$$(\{\tilde{\gamma}\}|is) = (\tilde{\gamma}|\{is\}) \qquad \text{collective} \tag{27}$$

$$K_{rs} = \sum_{\gamma i} (\{\tilde{\gamma}\}|is)(\{\tilde{\gamma}\}|is) \qquad \text{sum reduce } K_{rs} \tag{28}$$

$$C_\gamma = \sum_{si} (\{\tilde{\gamma}\}|is)C_{si} \qquad \text{sum reduce } C_\gamma \tag{29}$$

$$J_{rs} = \sum_\delta (\{\delta\}|rs) \sum_\gamma (\mathcal{J}^{-1/2})_{\delta\gamma}C_\gamma \qquad \text{sum reduce } J_{rs} \tag{30}$$

with $\mathcal{J}_{\gamma\delta} = (\gamma|\delta)$. The half index transformation (eq 24) and multiplication of $\mathcal{J}^{-1/2}$ in eq 26 only involves intranode operations and is threaded via the underlying BLAS calls. Similarly, computations of the exchange builds (eq 28) and the coulomb builds (eqs 29 and 30) are performed without communications, and the resulting two-index matrices are summed. The most communication-intensive steps are eqs 25 and 27, in which we need to collectively transpose the distributed three-index half-transformed integrals.

In our ASD algorithm, M monomer states are computed simultaneously in each diabatic subspace using Davidson diagonalization. The Davidson iteration requires one to compute

$$\sigma_J^{X,m} = \sum_{rs}\sum_I h_{rs}\langle J|\hat{E}_{rs}|I\rangle c_I^{X,m} + \frac{1}{2}\sum_{rstu}\sum_I (rs|tu)\langle J|\hat{E}_{rs,tu}|I\rangle c_I^{X,m} \tag{31}$$

for each state m in the quasi-diabatic sector X ($\hat{E}_{rs}$ and $\hat{E}_{rs,tu}$ are standard spin-free operators). Since, in our examples, M is greater than or equal to the number of MPI processes, this task can be trivially parallelized. The total wave functions are distributed to all the MPI processes; therefore, before each Davidson iteration, the $c^{X,m}$ are localized onto all the MPI processes. The M σ formations are split among all the MPI processes and each σ evaluation is performed locally. Our current implementation is sequential in X to minimize memory usage, making it scalable up to M MPI processes. For CAS wave functions, the evaluation of the two electron part of eq 31 is based on the algorithm proposed by Harrison and Zarrabian using $N_{\text{elec}} - 2$ electron intermediate determinants.[47] For RAS wave functions, we use the procedure proposed by Olsen et al.[34]

The wall times of a calculation of the singlet fission model Hamiltonian for the pentacene dimer[31] is presented as a function of the number of CPU cores in Figure 5. The total execution time, as well as the individual times for the most computationally expensive tasks—Hartree−Fock, monomer RAS(7,8,7)[1,1] calculations (22 active electrons), and Γ formations—are shown as a function of the number of CPU cores used. The most dominant portion of the calculation, by far, is Γ formation, comprising about two-thirds of the total computational time. Compared to using 64 CPU cores, parallelization of the Γ formation step leads to speed-ups by factors of 1.8, 2.5, and 2.9 for 128, 256, and 512 CPU cores, respectively. The deviation from the ideal speed-up (factors of 2, 4, and 8, respectively) is a result of the fact that, of the two main operations performed in the Γ formation (application of second quantization operators and formation of inner products between CI vectors), only the calculation of the inner product is parallelized across MPI processes. It is nonetheless worth noting that accurate modeling of chromophore dimers of materials interest using ASD can be routinely performed in an hour on a medium-sized computer cluster.

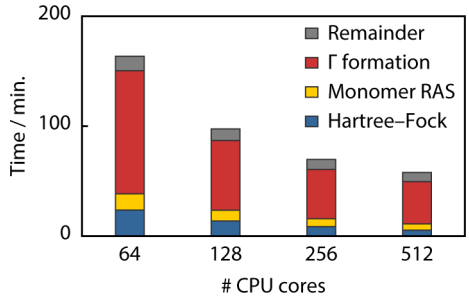

Figure 5. Computation times for singlet fission model Hamiltonian construction for the pentacene dimer (292 electrons) with the def2-TZVPP basis set[48] (1756 orbitals) using RAS(7,8,7)[1,1] with 22 active electrons to parametrize monomer wave functions and $M = 32$.

4. NUMERICAL EXAMPLES

In this section, we present model Hamiltonians for several charge- and energy-transfer processes in a benzene stack, and triplet excitation energy transfer in a benzene−naphthalene dimer.

Model Hamiltonians are defined by the dimer states used to build them and whether they involve only direct coupling or also mediated couplings (see eq 15). The dimer states are in turn defined by their diabatic character and by the number of states from each monomer, M, in which they are expanded. The "dimer space" refers to the full set of dimer states, i.e., the products of all charge- and spin-allowed combinations of monomer states, and may include types of monomer states not included in the model spaces. The portion of the dimer space not included in the model space is used only to compute mediated couplings.

According to Fermi's golden rule, the rate of an electronic transition is proportional to the squared magnitude of the electronic coupling between the initial and final states of the transition, H_{ij}. As a first example, we explore the distance dependence of these coupling matrix elements for several elementary electronic processes in a stacked benzene dimer: electron transfer (ET), hole transfer (HT), and triplet excitation energy transfer (TT). These processes are summarized in Figure 2.

ET and HT are described by the direct coupling between the initial and final states and thus are well-described by the direct model Hamiltonian. As both the benzene cation and anion have doubly degenerate ground states, we computed four-state model Hamiltonians: two states each of the type $|\Psi_{\pm 0}\rangle$ and $|\Psi_{0\pm}\rangle$. The four model states are thus $|\Psi^0_{\pm 0}\rangle$, $|\Psi^1_{\pm 0}\rangle$, $|\Psi^0_{0\pm}\rangle$ and $|\Psi^1_{0\pm}\rangle$, where the superscript labels the two degenerate solutions with the same diabatic character. We use the def2-TZVPP basis set[48] and $M = 32$ monomer states using CAS($6 - q$,6) wave functions, where q is the charge of the monomer. The resulting

dx.doi.org/10.1021/ct5004753 | J. Chem. Theory Comput. 2014, 10, 3738−3744

model Hamiltonian for ET in units of eV at a separation of 4.0 Å is

$$H^{\mathrm{ET}} = \begin{pmatrix} 0.000 & 0.000 & 0.372 & 0.000 \\ 0.000 & 0.000 & 0.000 & -0.372 \\ 0.372 & 0.000 & 0.000 & 0.000 \\ 0.000 & -0.372 & 0.000 & 0.000 \end{pmatrix} \begin{matrix} |\Psi^0_{-0}\rangle \\ |\Psi^1_{-0}\rangle \\ |\Psi^0_{0-}\rangle \\ |\Psi^1_{0-}\rangle \end{matrix} \quad (32)$$

This value for the coupling is similar to, but lower than, the value of 570 meV found by You et al.,[49] which was derived from the splittings of adiabatic states computed with spin-flip CI singles (estimated from Figure 4 of ref 49). Exploiting a property of symmetric homodimers, couplings can be inferred from adiabatic energy gaps through $\Delta E = 2H_{if}$. The model Hamiltonian for HT at a separation of 4.0 Å is

$$H^{\mathrm{HT}} = \begin{pmatrix} 0.000 & 0.000 & -0.248 & 0.000 \\ 0.000 & 0.000 & 0.000 & -0.248 \\ -0.248 & 0.000 & 0.000 & 0.000 \\ 0.000 & -0.248 & 0.000 & 0.000 \end{pmatrix} \begin{matrix} |\Psi^0_{+0}\rangle \\ |\Psi^1_{+0}\rangle \\ |\Psi^0_{0+}\rangle \\ |\Psi^1_{0+}\rangle \end{matrix} \quad (33)$$

This compares well with HT couplings of 214 meV from Kubas et al. derived from the splittings of adiabatic states computed with NEVPT2.[50]

For triplet energy transfer, by contrast, a mediated mechanism (also referred to as superexchange or through-configuration mechanisms) dominates.[43] In the mediated mechanism, triplet energy transfer can be considered simultaneous electron and hole transfers.[51] Thus, we compute two model Hamiltonians for TT: the direct (or Dexter transfer[52]) model Hamiltonian, which is computed in analogy to the ET and HT model Hamiltonians, and the mediated model Hamiltonian, which is computed using eq 15. In both cases, there are only two model states, since the triplet state of benzene is nondegenerate. The direct model Hamiltonian is

$$H^{\mathrm{TT}} = \begin{pmatrix} 0.000 & -0.009 \\ -0.009 & 0.000 \end{pmatrix} \begin{matrix} |\Psi_{\uparrow 0}\rangle \\ |\Psi_{0\uparrow}\rangle \end{matrix} \quad (34)$$

For the mediated model Hamiltonian, we use the charge transfer configurations $|\Psi_{+\,-}\rangle$ and $|\Psi_{-\,+}\rangle$ in the summation in eq 15. Then, the mediated model Hamiltonian for TT at 4.0 Å is

$$\tilde{H}^{\mathrm{TT}} = \begin{pmatrix} 0.000 & 0.026 \\ 0.026 & 0.000 \end{pmatrix} \begin{matrix} |\tilde{\Psi}_{\uparrow 0}\rangle \\ |\tilde{\Psi}_{0\uparrow}\rangle \end{matrix} \quad (35)$$

The magnitudes of all the coupling elements as a function of separation are shown in Figure 6.

The ASD method, unlike methods based on the energetic splitting of adiabatic eigenstates, is not limited to homodimers. To demonstrate, we computed triplet transfer model Hamiltonians for a benzene−naphthalene dimer stack separated by 3.5 Å. Calculations used def2-TZVPP for the basis set, CAS($6-q$,6) for the benzene monomer states and CAS($10-q$,10) for the naphthalene monomer states, all with $M = 32$. The resulting mediated Hamiltonian is

$$\tilde{H}^{\mathrm{TT}} = \begin{pmatrix} 0.000 & 0.0038 \\ 0.0038 & -1.01 \end{pmatrix} \begin{matrix} |\tilde{\Psi}_{B^{\uparrow}N^{0}}\rangle \\ |\tilde{\Psi}_{B^{0}N^{\uparrow}}\rangle \end{matrix} \quad (36)$$

where $|\tilde{\Psi}_{B^{\uparrow}N^{0}}\rangle$ and $|\tilde{\Psi}_{B^{0}N^{\uparrow}}\rangle$ denote the states in which the triplet resides on the benzene and the naphthalene, respectively. Similarly, our recently reported model Hamiltonians for singlet fission in tetracene and pentacene dimers built from experimental crystal structures demonstrates that ASD can efficiently treat asymmetric dimers.[31]

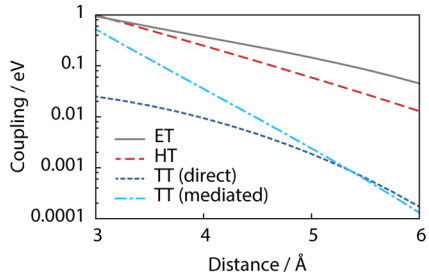

Figure 6. Exponential decay of the coupling elements for ET, HT, direct TT, and mediated TT in a stacked benzene dimer (see main text). Calculations used def2-TZVPP basis set,[48] with CAS($6-q$,6) monomer states (with charge q) and $M = 32$.

5. CONCLUSIONS

We have presented the active space decomposition method in which a system's wave function is written as a sum of products of fragment wave functions. ASD borrows conceptually from the matrix product states of DMRG and from traditional quantum chemistry wave function ansätze. Within ASD, Hamiltonian matrix elements can be computed entirely in terms of fragment transition density tensors, leading to significant computational advantages since the full space is never explicitly constructed. Since it requires only transition density matrices between fragment states, ASD is compatible with any fragment wave function method for which transition density matrices can be efficiently computed. We have focused on active space methods, in particular the CAS and RAS methods.

In addition, we have shown that the quasi-diabatic framework of ASD makes it readily applicable to the computation of model Hamiltonians for electronic processes in molecular dimers, in which each molecular unit of the dimer is considered a fragment. Thus, ASD facilitates interpretation of electronic processes while enabling large-scale calculations that would be otherwise prohibitive. We demonstrated this by computing direct and mediated model Hamiltonians for electron, hole, and triplet energy transfers in a stacked benzene dimer, and for triplet energy transfer in a benzene−naphthalene dimer.

The dominant portion of an ASD calculation is the formation of the transition density tensors, Γ. By casting the formation of Γ in terms of a tree structure, we developed an efficient parallel algorithm that makes use of intermediate quantities. This parallel algorithm enables us to accurately calculate model Hamiltonians for electronic processes in chromophores of materials interest in a medium sized compute cluster in about an hour. All methods discussed here have been implemented in BAGEL, an open-source quantum chemistry code.[32] Orbital optimization and dynamical correlation treatment based on the ASD method will be considered in future work.

AUTHOR INFORMATION

Corresponding Authors

*E-mail: shane.parker@u.northwestern.edu (S. M. Parker).

*E-mail: shiozaki@northwestern.edu (T. Shiozaki).

Notes

The authors declare no competing financial interest.

■ ACKNOWLEDGMENTS

This work has been supported by Office of Basic Energy Sciences, U.S. Department of Energy (Grant No. DE-FG02-13ER16398). S.M.P. thanks Profs. Mark Ratner and Tamar Seideman for encouragement.

■ REFERENCES

(1) Helgaker, T.; Jørgensen, P.; Olsen, J. *Molecular Electronic-Structure Theory*; Wiley: West Sussex, U.K., 2000.
(2) Christiansen, O.; Jørgensen, P.; Hättig, C. *Int. J. Quantum Chem.* **1998**, *68*, 1−52.
(3) Riplinger, C.; Neese, F. *J. Chem. Phys.* **2013**, *138*, 034106.
(4) Nakatsuji, H. *Acc. Chem. Res.* **2012**, *45*, 1480−1490.
(5) Mitroy, J.; Bubin, S.; Horiuchi, W.; Suzuki, Y.; Adamowicz, L.; Cencek, W.; Szalewicz, K.; Komasa, J.; Blume, D.; Varga, K. *Rev. Mod. Phys.* **2013**, *85*, 693−749.
(6) Mead, C. A.; Truhlar, D. G. *J. Chem. Phys.* **1982**, *77*, 6090−6098.
(7) Heumann, B.; Schinke, R. *J. Chem. Phys.* **1994**, *101*, 7488−7499.
(8) Pacher, T.; Cederbaum, L. S.; Köppel, H. *J. Chem. Phys.* **1988**, *89*, 7367−7381.
(9) Domcke, W.; Woywod, C. *Chem. Phys. Lett.* **1993**, *216*, 362−368.
(10) Simah, D.; Hartke, B.; Werner, H.-J. *J. Chem. Phys.* **1999**, *111*, 4523−4534.
(11) Subotnik, J. E.; Cave, R. J.; Steele, R. P.; Shenvi, N. *J. Chem. Phys.* **2009**, *130*, 234102.
(12) Subotnik, J. E.; Vura-Weis, J.; Sodt, A. J.; Ratner, M. A. *J. Phys. Chem. A* **2010**, *114*, 8665−8675.
(13) Dederichs, P. H.; Blugel, S.; Zeller, R.; Akai, H. *Phys. Rev. Lett.* **1984**, *53*, 2512−2515.
(14) Wu, Q.; Van Voorhis, T. *Phys. Rev. A* **2005**, *72*, 024502.
(15) Kaduk, B.; Kowalczyk, T.; Van Voorhis, T. *Chem. Rev.* **2012**, *112*, 321−370.
(16) Difley, S.; Van Voorhis, T. *J. Chem. Theory Comput.* **2011**, *7*, 594−601.
(17) Mo, Y.; Gao, J. *J. Phys. Chem. A* **2000**, *104*, 3012−3020.
(18) Wu, W.; Su, P.; Shaik, S.; Hiberty, P. C. *Chem. Rev.* **2011**, *111*, 7557−7593.
(19) Fink, R. F.; Pfister, J.; Schneider, A.; Zhao, H.; Engles, B. *Chem. Phys.* **2008**, *343*, 353−361.
(20) Havenith, R. W. A.; de Gier, H. D.; Broer, R. *Mol. Phys.* **2012**, *110*, 2445−2454.
(21) Malmqvist, P.-Å. *Int. J. Quantum Chem.* **1986**, *30*, 479−494.
(22) Al Hajj, M.; Malrieu, J.-P.; Guihéry, N. *Phys. Rev. B* **2005**, *72*, 224412.
(23) Zhang, H.; Malrieu, J.-P.; Ma, H.; Ma, J. *J. Comput. Chem.* **2011**, *33*, 34−43.
(24) Ma, Y.; Liu, Y.; Ma, H. *J. Chem. Phys.* **2012**, *136*, 024113.
(25) Ma, Y.; Ma, H. *J. Phys. Chem. A* **2013**, *117*, 3655−3665.
(26) Abramavicius, D.; Palmieri, B.; Voronine, D. V.; Šanda, F.; Mukamel, S. *Chem. Rev.* **2009**, *109*, 2350−2408.
(27) Morningstar, C. J.; Weinstein, M. *Phys. Rev. Lett.* **1994**, *73*, 1873−1877.
(28) Morningstar, C. J.; Weinstein, M. *Phys. Rev. D* **1996**, *54*, 4131−4151.
(29) Malrieu, J.-P.; Guihéry, N. *Phys. Rev. B* **2001**, *63*, 085110.
(30) Parker, S. M.; Seideman, T.; Ratner, M. A.; Shiozaki, T. *J. Chem. Phys.* **2013**, *139*, 021108.
(31) Parker, S. M.; Seideman, T.; Ratner, M. A.; Shiozaki, T. *J. Phys. Chem. C* **2014**, *118*, 12700−12705.
(32) BAGEL, Brilliantly Advanced General Electronic-structure Library; available via the Internet at http://www.nubakery.org, under the GNU General Public License.
(33) Nakano, H.; Hirao, K. *Chem. Phys. Lett.* **2000**, *317*, 90−96.
(34) Olsen, J.; Roos, B. O.; Jørgensen, P.; Jensen, H. J. A. *J. Chem. Phys.* **1988**, *89*, 2185−2192.
(35) Ivanic, J. *J. Chem. Phys.* **2003**, *119*, 9364−9376.
(36) Ma, D.; Manni, G. L.; Gagliardi, L. *J. Chem. Phys.* **2011**, *135*, 044128.
(37) White, S. R. *Phys. Rev. Lett.* **1992**, *69*, 2863−2866.
(38) Schollwöck, U. *Ann. Phys.* **2011**, *326*, 96−192.
(39) Chan, G. K.-L.; Sharma, S. *Annu. Rev. Phys. Chem.* **2011**, *62*, 465−481.
(40) Kurashige, Y.; Yanai, T. *J. Chem. Phys.* **2009**, *130*, 234114.
(41) Zgid, D. Private communcations; Chan, G. K.-L. Private communcations.
(42) Chan, G. K.-L. *WIRES—Comput. Mol. Sci.* **2012**, *2*, 907−920.
(43) Harcourt, R. D.; Scholes, G. D.; Ghiggino, K. P. *J. Chem. Phys.* **1994**, *101*, 10521−10525.
(44) Berkelbach, T. C.; Hybertsen, M. S.; Reichman, D. R. *J. Chem. Phys.* **2013**, *138*, 114103.
(45) Bloch, C. *Nucl. Phys.* **1958**, *6*, 329−347.
(46) Nakano, H. *J. Chem. Phys.* **1993**, *99*, 7983−7992.
(47) Harrison, R. J.; Zarrabian, S. *Chem. Phys. Lett.* **1989**, *158*, 393−398.
(48) Weigend, F.; Ahlrichs, R. *Phys. Chem. Chem. Phys.* **2005**, *7*, 3297−3305.
(49) You, Z.-Q.; Shao, Y.; Hsu, C.-P. *Chem. Phys. Lett.* **2004**, *390*, 116−123.
(50) Kubas, A.; Hoffmann, F.; Heck, A.; Oberhofer, H.; Elstner, M.; Blumberger, J. *J. Chem. Phys.* **2014**, *140*, 104105.
(51) Closs, G. L.; Johnson, M. D.; Miller, J. R.; Piotrowiak, P. *J. Am. Chem. Soc.* **1989**, *111*, 3751−3753.
(52) Dexter, D. L. *J. Chem. Phys.* **1953**, *21*, 836−850.